Fabrication of electrically conductive poly(styrene-b-ethylene-ran-butylene-b-styrene)/multi-walled carbon nanotubes composite fiber and its application in ultra-stretchable strain sensor

Lele Li [a], Zikai Du [a], Baojie Sun [a], Wenyue Li [b], Liang Jiang [a,*], Yanfen Zhou [a,*], Jianwei Ma [a], Shaojuan Chen [a], Feng-Lei Zhou [a, c]

[a] College of Textiles and Clothing, Qingdao University, Qingdao, 266071, China

[b] College of Materials Science and Engineering, Beijing University of Chemical Technology, Beijing, 100029, China

[c] Centre for Medical Image Computing, University College London, London, WC1V 6LJ, UK

* Corresponding author: liang.jiang@qdu.edu.cn (Liang Jiang); yanfen.zhou@qdu.edu.cn (Yanfen Zhou)

ABSTRACT

Although flexible polymer composites based strain sensors have been widely studied, it is still a challenge to obtain flexible strain sensors with large working range, high sensitivity and reliable stability. In this research, a flexible strain sensor based on poly(styrene-b-ethylene-ran-butylene-b-styrene) (SEBS)/multi-walled carbon nanotubes (MWCNTs) composite fiber was prepared through the wet spinning method. In particular, the effects of MWCNTs content and aspect ratio (L/D) on the morphology, and mechanical, electrical and electromechanical properties of the composite fiber were studied. The results showed that with the increase of MWCNTs content, the tensile strength and elongation at break of the composite fiber decreased, while the electrical conductivity and the strain sensing range increased. For the same MWCNTs content, the composite fiber filled with MWCNTs of the lowest L/D ratio (1.25/15) showed the highest tensile strength and elongation at break; whereas the composite fiber filled with

MWCNTs of the highest L/D ratio (20/15) showed the highest electrical conductivity, strain sensing range (0-506%) and sensitivity (gauge factor of 58.274 at 0% - 275% strain, and of 197.944 at 275% - 506% strain). The fabricated composite fiber could be formed into a knitted fabric and had the ability of detecting various human motions.

Keywords: Fiber; Electrically conductive; Strain sensing

1. Introduction

Smart wearable technology, which can integrate all kinds of perception, recognition, connection and cloud services into daily wearable devices to realize the functions of human senses, intelligent housekeeper, social entertainment, health monitoring, etc., has attracted extensive attention.[1, 2] As an important part of intelligent wearable, strain sensors have been widely used to measure physiological and physical signals generated by human body,[3, 4] and have also become an important tool for disease diagnosis,[5] treatment and health monitoring.[6] Traditionally, metal and semiconductor materials had been used for strain sensors,[7, 8] but their flexibility, ductility and detection range are greatly limited. To meet the requirements of flexible strain sensors, conductive polymer composites,[9] which overcome the shortcomings of traditional strain sensors and have the advantages of good extensibility,[10] lightweight and wearability, have received increasing attention.[11-14] In particular, conductive polymer fibers with weaveability have been developed rapidly for application in strain sensors in recent years. Various polymers, including thermoplastic polyurethane (TPU),[15] styrene-butene-styrene copolymer (SBS),[16] and so on, have been selected as the matrix for fabricating fiber based strain sensors.[17-19] For example, Li et al. fabricated a kind of fiber-shaped strain sensor based on electrospinning TPU nanofiber yarns dipped with multi-walled carbon nanotubes (MWCNTs) and single-walled carbon nanotubes (SWCNTs), respectively. This strain sensor showed a working range of 0–100%, reliable stability during 2000

stretching-releasing cycles, but the gauge factor ($GF = \Delta R/(R_0 \cdot \varepsilon)$, $\Delta R=R-R_0$, R is the instantaneous resistance, R_0 is the initial resistance, ε is strain) was below 2 in the strain range of 0–100%.[20]

The selection of a suitable conductive component has an important influence on the performance of flexible strain sensors.[21] At present, the conductive materials of flexible sensors mainly include metal nanomaterials (metal nanowires, nanorods and nanoparticles),[22-24] CNTs,[16, 25] graphene[26, 27] and their hybrids.[28, 29] The conductive fillers could be coated on the surface of the polymer matrix or dispersed inside the polymer matrix.[30-32] Among various conductive components, CNTs have the advantages of excellent conductivity, good mechanical properties and good stability and have been widely used in the fabrication of flexible strain sensors.[26] For example, Wang et al. fabricated TPU/MWCNTs fiber based strain sensor by utilizing the wet spinning method. This strain sensor had a working strain range of 320%, a relatively high GF of 22.2 within 160% strain and 97.1 in the strain range of 160–320%.[33]

Although CNTs have been widely used in the fabrication of strain sensors, the effect of CNTs aspect ratio (L/D) on the sensing performance of fiber-based strain sensors is still unclear. In this work, conductive composite fiber based on poly(styrene-b-ethylene-ran-butylene-b-styrene) (SEBS) and MWCNTs was fabricated through a simple wet spinning process. The effects of MWCNTs aspect ratio and content on the morphology and mechanical, electrical, and electromechanical property of the composite fiber were investigated. SEBS/MWCNTs fiber with electrical conductivity as high as 0.00686 S/cm was obtained when the L/D of the MWCNTs was 20/15 and the mass fraction was 5%. The SEBS/MWCNTs composite fiber could sense large strains of up to 506% with a high GF of 58.274 at 0% - 275% strain, and of 197.944 at 275% - 506% strain. The excellent mechanical properties of SEBS/MWCNTs composite fibers enabled their

knitting into textiles. The strain sensors based on the SEBS/MWCNTs composite fibers and their knitted fabric can be used in monitoring various human body motions, including the neck, hand, wrist, elbow and knee bendings.

2. Experimental Section

2.1. Materials

SEBS with Shore A hardness of 60 (10 seconds, molding), styrene/rubber ratio of 33/67 and density of 0.910 g/cm^3 was purchased from Kraton, USA. MWCNTs were purchased from Xianfeng nanomaterials technology Co., Ltd (Jiangsu, China). Three kinds of MWCNTs with different L/D ratios were used: length 10-30 μm, diameter 10-20 nm, denoted as MWCNTs-20/15 (purity >95%); length 0.5-2 μm, diameter 10-20 nm, denoted as MWCNTs-1.25/15 (purity >95%); length 0.25-2 μm, diameter 4-6 nm, denoted as MWCNTs-1.25/5 (purity >98%). Tetrahydrofuran (THF, 99.5%) and anhydrous ethanol were purchased from Sinopharm Chemical Reagent Co., Ltd. (Shanghai, China).

2.2. Fabrication of SEBS/MWCNTs Composite Fiber

The process for preparing SEBS/MWCNTs composite fiber is shown schematically in Figure 1. Firstly, a certain amount of MWCNTs was dispersed in THF (15 ml) and dispersed under ultrasonication for 2 h (every 15 min, stop 5 min, repeat 6 times). Then, a specific amount of SEBS was added into the mixed suspension of THF and MWCNTs (SEBS and MWCNTs always accounted for 25 wt% of SEBS, MWCNTs and THF), stirred magnetically for 18 h at ambient condition and treated under ultrasonication for 1 h followed by magnetic stirring for another 1 h. Finally, the SEBS/MWCNTs conductive composite fibers were prepared through wet spinning and dried in vacuum at 30 °C for 12 h to ensure complete removal of the solvent. A 23G needle with inner and outer diameter of 0.33 mm and 0.63 mm respectively was used, and the extrusion

rate of the spinning solution was 1.7 ml/h. Anhydrous ethanol was used as coagulation bath. The fibers fabricated by using different content of MWCNTs-20/15, MWCNTs-1.25/15 and MWCNTs-1.25/5 were represented by SEBS/xMWCNTs-20/15, SEBS/xMWCNTs-1.25/15 and SEBS/xMWCNTs-1.25/5 respectively, where x represents the mass ratio of MWCNTs in the SEBS/MWCNTs composite fiber. For example, SEBS/2%MWCNTs-20/15 denotes for the composite fibers containing 2 wt% MWCNTs-20/15.

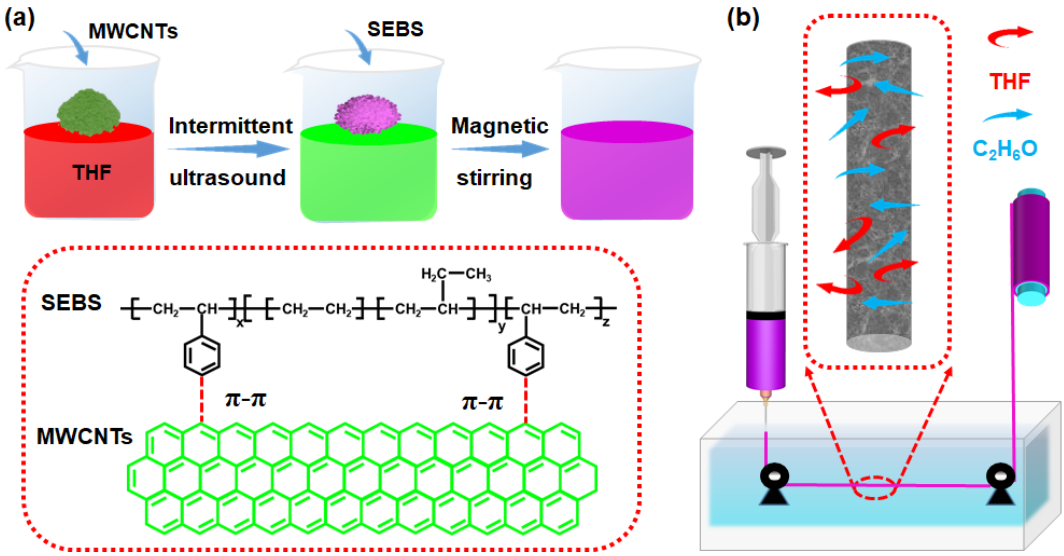

Figure 1. Schematic illustration for preparing SEBS/MWCNTs composite fibers.

2.3. Characterization

The longitudinal surface and cross section of fibers were observed by employing a scanning electron microscope (SEM, Tescan Vega3, Czech). Samples for cross-sectional observation were frozen in liquid nitrogen and broken manually. The samples were coated with gold for 60 s before observation and SEM images were taken at an accelerating voltage of 10 kV. The Raman spectra was performed by using an intelligent Raman microscope (Thermo Scientific DXR2, America) in the range of 400-4000 cm^{-1} at 1 cm^{-1} resolution with 532 nm laser excitation. The mechanical properties of the fibers were tested by employing an universal testing machine (Instron 5965, United

States). Single fibers with a clamping distance of 20 mm were used and the tensile speed was controlled at 100 mm/min. At least five tests were conducted for each sample and the average tensile strength and elongation at break were used. A TG/DSC thermal analyzer (STA449 F3 Jupiter, Bavaria, Germany) was used to analyze the thermal behaviour of the fiber. The measurement were conducted in the temperature range of 40-800 °C with a heating rate of 20 °C/min. A precision power supply (B2901A Keysight, USA) was used to test the electrical resistance and the piezoresistive behavior of the composite fibers. For piezoresistive behavior test, two ends of the fiber were wrapped with copper strips and clamped on the stepping motor with a clamping distance of 10 mm, the stretching speed was controlled at 10 mm/min, the precision power supply was connected with the sample through wires, and the computer was connected with the precision power supply to record the real time change of electrical resistance.

3. Results and Discussion

3.1. Morphology, Raman Spectroscopy and Thermal Stability

Figure 2 shows the surface and cross-section morphology of the SEBS/MWCNTs fibers fabricated by using MWCNTs with different L/D ratios. It can be seen that the surface of the fibers was rough and granular (Figure 2a, c and e), the cross section showed a 'bean' shape (Figure 2b, d and f) due to the shrinking of fiber during the solidification process.[27] Compared with SEBS/5%MWCNTs-1.25/15 fiber (Figure 2d), more MWCNTs aggregates (as marked by red dotted circles) could be observed clearly inside the SEBS/5%MWCNTs-20/15 (Figure 2b) and SEBS/5%MWCNTs-1.25/5 (Figure 2f) fibers, indicating that MWCNTs of a lower L/D ratio had better dispersion in the SEBS matrix.

Porous structure could also be observed from the cross-sectional morphology of the composite fibers. Notably, the porous structure was more obvious closer to the fiber

center (Figure 2g). In addition, the higher the content of MWCNTs in the fiber, the less obvious the porous structure (Figure 2f, h). These phenomena can be explained by the solvent exchange during the wet spinning process. In the solidification stage, the solvent contained in the fibers diffused into the coagulation bath and simultaneously the coagulation liquid diffused into the fibers. The fiber surface solidified firstly, which inhibited the solvent exchange at the core of the fiber.[34] For SEBS/MWCNTs composite fiber with a higher CNTs loading, more CNTs provided more channels for solvent exchange, so the formed porous structure was less obvious.

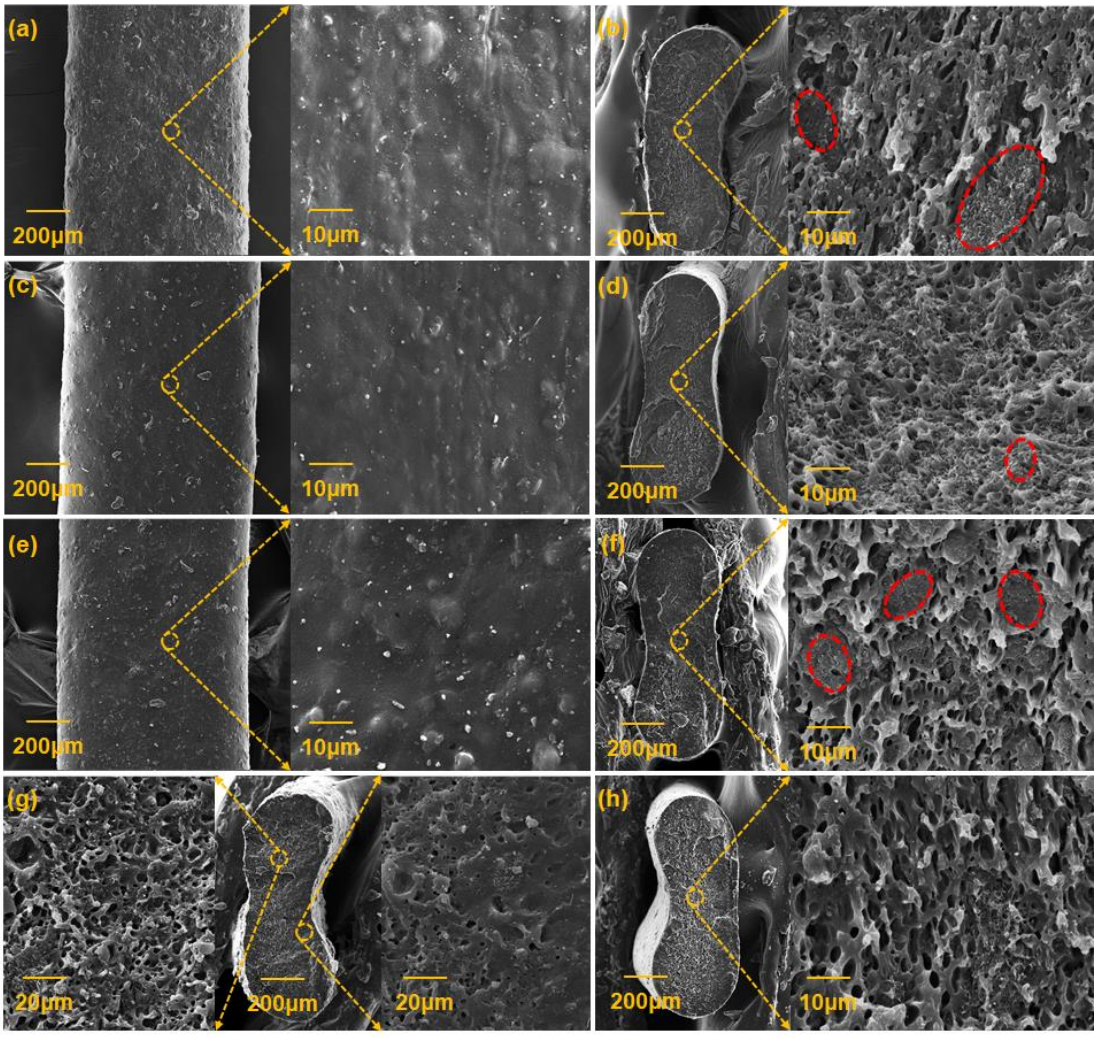

Figure 2. SEM image of SEBS/MWCNTs composite fiber. The longitudinal surface and cross section of (a, b) SEBS/5%MWCNTs-20/15, (c, d) SEBS/5%MWCNTs-1.25/15, (e, f) SEBS/5%MWCNTs-1.25/5; (g) the center and edge of cross section of

SEBS/2%MWCNTs-1.25/5; (h) cross section of SEBS/2%MWCNTs-1.25/5.

Raman spectroscopy was used to determine the carbon structure and possible interactions between MWCNTs and the SEBS matrix. Figure 3a and b show the Raman spectroscopy of MWCNTs-20/15, MWCNTs-1.25/15, MWCNTs-1.25/5 and their SEBS composites with the MWCNTs content of 5%. It can be seen from Figure 3a that MWCNTs-20/15, MWCNTs-1.25/15 and MWCNTs-1.25/5 showed typical D bands at 1346.3 cm^{-1}, 1343.4 cm^{-1}, 1340.5 cm^{-1} and G bands at 1579.7 cm^{-1}, 1578.5 cm^{-1}, 1578.5 cm^{-1}, respectively. In general, a higher I_D/I_G ratio (I_D and I_G are the strengths of D and G bands) indicates more defects in MWCNTs.[34-36] The I_D/I_G of MWCNTs-20/15, MWCNTs-1.25/15 and MWCNTs-1.25/5 was 0.852, 0.851 and 0.849, respectively. These results suggested that sp^3 defects might exist in the sp^2 carbon network of MWCNTs.[34, 37]

Compared with MWCNTs, the peak center of D band for SEBS/5%MWCNT-20/15, SEBS/5%MWCNT-1.25/15 and SEBS/5%MWCNT-1.25/5 showed a shift of 4.9 cm^{-1} (from 1346.3 cm^{-1} to 1351.2 cm^{-1}), 7.1 cm^{-1} (from 1343.4 cm^{-1} to 1350.5 cm^{-1}) and 5.9 cm^{-1} (from 1340.5 cm^{-1} to 1346.4 cm^{-1}), respectively. This indicates there was non-covalent $\pi-\pi$ interactions between MWCNTs and the aromatic rings of PS of the SEBS matrix.[37, 38] The I_D/I_G ratios of SEBS/5%MWCNTs-20/15, SEBS/5%MWCNTs-1.25/15 and SEBS/5%MWCNTs-1.25/5 was 0.851, 0.854 and 0.848 respectively. Compared with MWCNTs, The I_D/I_G ratio of SEBS/MWCNTs changed little, indicating that the preparation process had little effect on the defects of MWCNTs.[38]

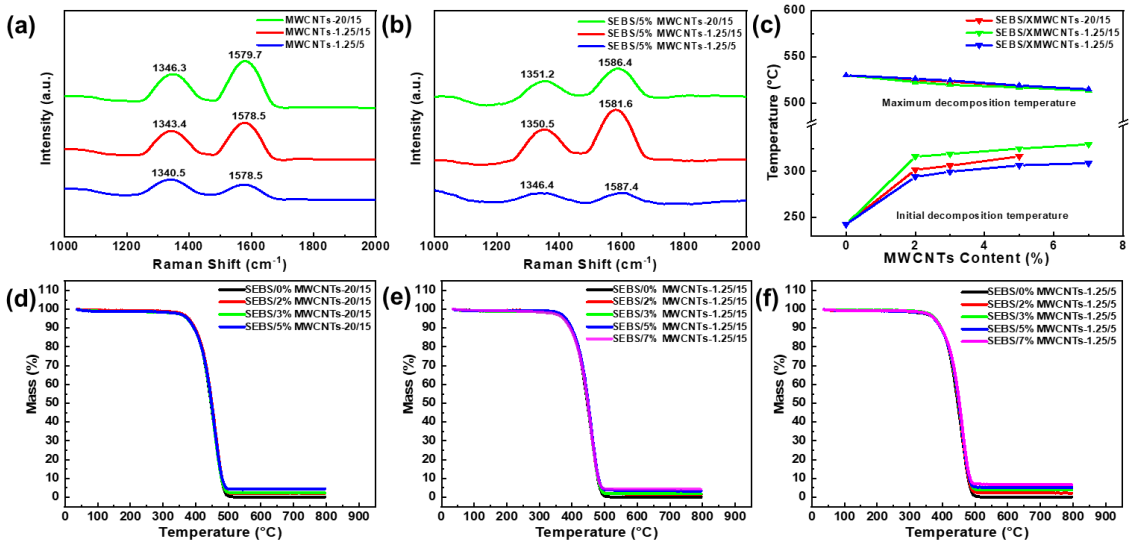

Figure 3. (a-b) Raman spectra of MWCNTs-20/15, MWCNTs-1.25/15, MWCNTs-1.25/5 and SEBS/5%MWCNTs-20/15, SEBS/5%MWCNTs-1.25/15, SEBS/5%MWCNTs-1.25/5; (c) Initial decomposition temperature and maximum decomposition temperature of different SEBS/MWCNTs fibers; (d-f) TG curves of SEBS and SEBS/xMWCNTs-20/15, SEBS/xMWCNTs-1.25/15, SEBS/xMWCNTs-1.25/5 fibers.

Thermal stability of the composite fiber was investigated through thermogravimetric analysis. Figure 3d-f show the TG curves of SEBS and SEBS/MWCNTs composite fibers. It can be seen that the thermal decomposition process of SEBS fiber and SEBS/MWCNTs composite fibers was almost the same. The decomposition temperature of the fiber was calculated, as shown in Figure 3c. The initial and maximum decomposition temperatures of pure SEBS fiber were 242.44 °C and 530.05 °C respectively. With the addition of MWCNTs, the initial decomposition temperature of the fiber increased, the maximum decomposition temperature decreased, and the decomposition process of the fiber was shortened. This is because the thermal conductivity of carbon nanotubes was up to 3000 W/MK, which could transfer heat to the inner layer of the composite fiber and accelerate the decomposition of the fiber.[39]

3.2. Mechanical and Electrical Properties

Figure 4a-c show the stress-strain curves of SEBS/MWCNTs fibers filled with MWCNTs of different L/D ratios, the average values of tensile strength and elongation at break are shown in Figure 4d-f. The tensile strength and elongation at break of pure SEBS fiber were 50.46 ± 1.44 MPa and 1626.68 ± 30.00%, respectively. The addition of MWCNTs decreased the tensile strength and elongation of SEBS fiber. It can be seen that for SEBS/MWCNTs fibers filled with the same kind of MWCNTs, the tensile strength and elongation at break decreased with the increase of MWCNTs content. This is because when the content of MWCNTs was high, the strong van der Waals force between them led to serious agglomeration and limited the movement of SEBS molecular chain.[40]

When the MWCNTs content was the same, SEBS/MWCNTs-1.25/15 showed the highest tensile strength and elongation at break. This is because MWCNTs-1.25/15 with the lowest aspect ratio had enhanced mobility during dispersion inside the polymer matrix.[41] Compared with MWCNT-1.25/5, the MWCNT-20/15 had both longer length and larger diameter. Longer nanotubes are in favor of the formation of polymer-MWCNT network through bridging the neighboring polymer and the formation of CNTs network through entanglement, thus increasing the mechanical properties of the composite fiber.[42] The elongation at break of all conductive composite fibers was higher than 800% and the tensile strength was higher than 30 MPa, which were suitable for manufacturing strain sensors in terms of elongation at break and tensile strength.

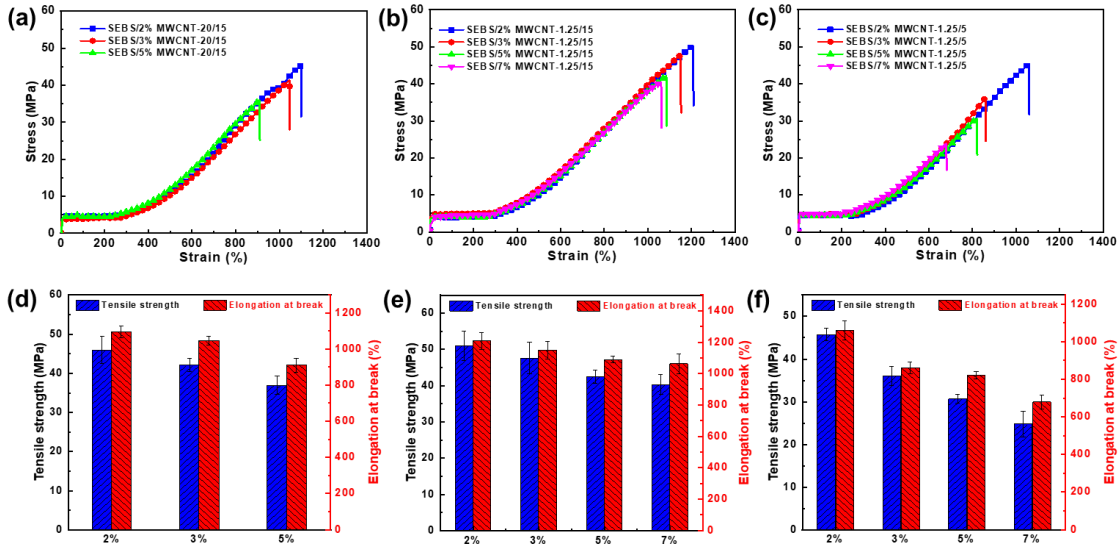

Figure 4. Mechanical properties of SEBS/xMWCNTs composite fibers. (a-c) Stress-strain curves of SEBS/xMWCNTs-20/15, SEBS/xMWCNTs-1.25/15, SEBS/xMWCNTs-1.25/5 in order; (d-f) Tensile strength and elongation at break of SEBS/xMWCNTs-20/15, SEBS/xMWCNTs-1.25/15, SEBS/xMWCNTs-1.25/5 in order.

Figure 5a shows the electrical conductivity of SEBS/MWCNTs composite fibers. From Figure 5a it can be seen that, for each kind of MWCNTs used, the conductivity of the composite fiber increased with the increase of MWCNTs mass fraction. Except for the CNTs content, the electrical conductivity of CNTs filled polymer composites is also reported to be related to the intrinsic conductivity of the CNTs, the dispersion and dimensions of CNTs.[43] As known from the Raman spectroscopy, the I_D/I_G ratios of MWCNTs-20/15, MWCNTs-1.25/15 and MWCNTs-1.25/5 were quite close, indicating similar structural qualities and intrinsic electrical conductivity of these MWCNTs.[42] A higher aspect ratio generally lead to a lower percolation threshold and better electrical conductivity, because CNTs with a higher aspect ratio would form a better conductive CNT network inside of polymer.[44] It can be seen from Figure 5a that when the MWCNTs content was the same, the conductivity of SEBS/xMWCNTs-20/15 was

higher than SEBS/xMWCNTs-1.25/15 because of the better MWCNTs network formed. It can also be seen that the conductivity of SEBS/xMWCNTs-1.25/15 was higher than that of SEBS/xMWCNTs-1.25/5 when the MWCNTs content was the same. This is because the larger the diameter of the MWCNTs, the easier they were to contact along the diameter direction, forming a conductive path.[45] The conductivity increased dramatically when the content of the filler reached the electrical percolation threshold.[46] The percolation thresholds of SEBS/xMWCNTs-20/15, SEBS/xMWCNTs-1.25/15, SEBS/xMWCNTs-1.25/5 was 1.52524, 2.58892 and 2.24747, respectively (Figure 5b-d).

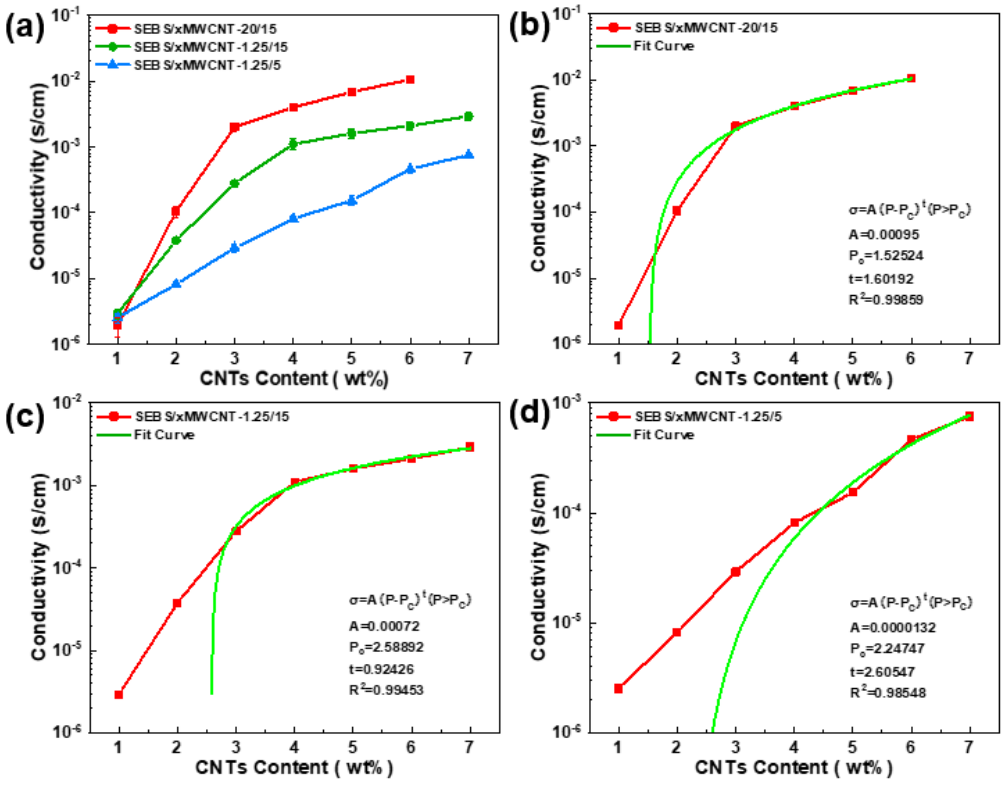

Figure 5. (a) The effect of MWCNTs content on conductivity of SEBS/xMWCNTs-20/15, SEBS/xMWCNTs-1.25/15, SEBS/xMWCNTs-1.25/5; Fit curves of (b) SEBS/xMWCNTs-20/15, (c) SEBS/xMWCNTs-1.25/15 and (d) SEBS/xMWCNTs-1.25/5.

3.3. Piezoresistive Performance

The piezoresistive performance of SEBS/MWCNTs composite fibers with MWCNTs of different L/D aspect ratios was investigated. Figure 6a-c show the change of relative resistance ($\Delta R/R_0$, where $\Delta R=R-R_0$, R is the instantaneous resistance, R_0 is the initial resistance) with increasing strain for SEBS/MWCNTs composite fibers. For SEBS/MWCNTs composite fibers with the same type of MWCNTs, the strain sensing range increased with increasing MWCNTs content. For example, the strain sensing range of SEBS/3%MWCNTs-20/15 was 0-72%, while it was 0-506% for SEBS/5%MWCNTs-20/15. When making a comparison between SEBS/MWCNTs composite fibers with MWCNTs of different L/D aspect ratios, it was found that for the same MWCNTs content, the strain sensing range of SEBS/MWCNTs-20/15 (0-506%) was higher than that of SEBS/MWCNTs-1.25/15 (0-81%), while the strain sensing range of SEBS/MWCNTs-1.25/15 was higher than that of SEBS/MWCNTs-1.25/5 (0-11%). This is because the better conductive network formed by MWCNTs with longer length and larger diameter need larger deformation to be broken.

GF was employed to characterize the sensitivity and linearity of the composite fibers. Figure 6e showed that the electrical response characteristics of SEBS/7%MWCNTs-1.25/15 could be divided into three linear regions: GF_1 of 22.873 at 0% - 15% strain, GF_2 of 74.498 at 15% - 80% strain, and GF_3 of 21.587 at 80% - 180% strain. The electrical response characteristics of SEBS/5%MWCNTs-20/15 could be divided into two linear regions: GF_1 of 58.274 at 0% - 275% strain and GF_2 of 197.944 at 275% - 506% (Figure 6d). SEBS/7%MWCNTs-1.25/5 had GF_1 of 13.700 at 0% - 170% strain. Compared with SEBS/MWCNTs-1.25/15 and SEBS/MWCNTs-1.25/5 composite fiber, the strain sensor based on SEBS/MWCNTs-20/15 had wider strain sensing range and high sensitivity, which is better than recently reported strain sensors (Figure 6g).

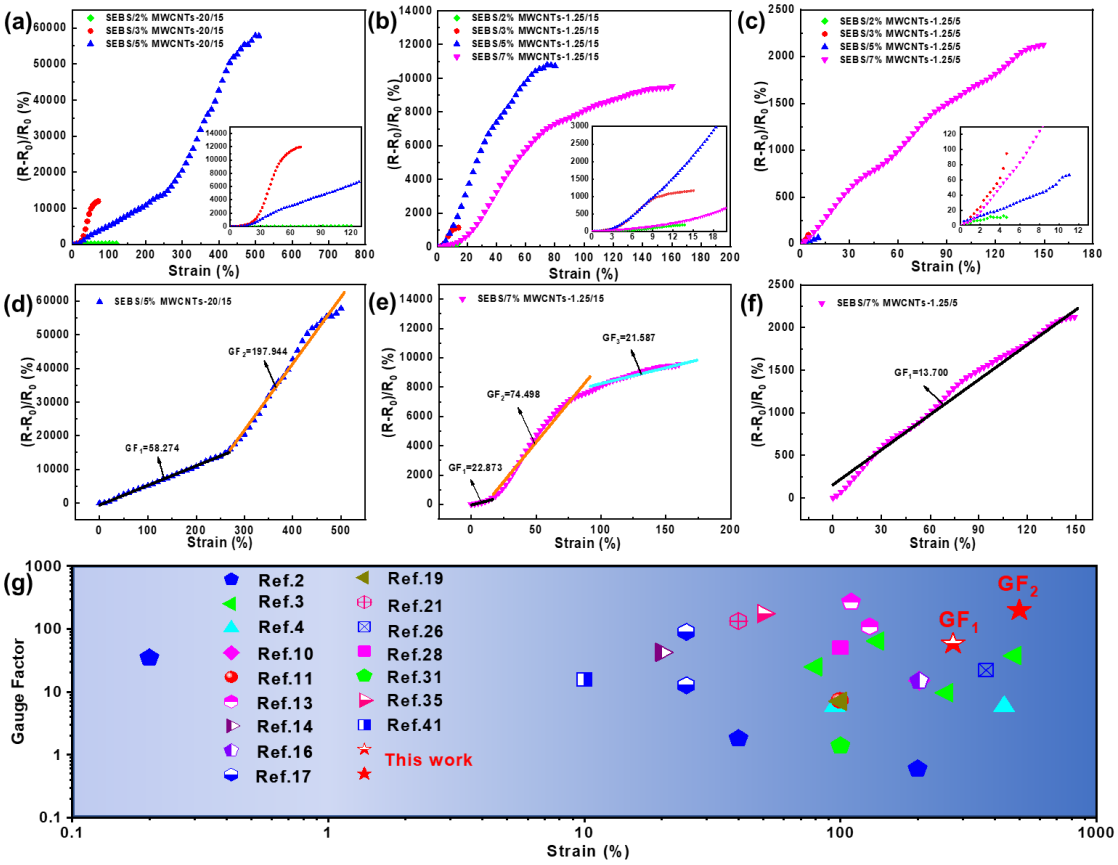

Figure 6. (a-c) The $\Delta R/R_0$-strain curves of SEBS/xMWCNTs-20/15, SEBS/xMWCNTs-1.25/15, SEBS/xMWCNTs-1.25/5; (d-f) The detailed sensitivity and linear behavior of SEBS/5%MWCNTs-20/15, SEBS/7%MWCNTs-1.25/15, SEBS/7%MWCNTs-1.25/5 strain sensors; (g) Comparison of GF and maximum workable range of SEBS/5%MWCNTs-20/15 strain sensor with those of recently reported piezoresistive strain sensors.

The dynamic strain sensing behavior was investigated. Figure 7a-c shows respectively the dynamic response behavior of the strain sensor based on SEBS/5%MWCNTs-20/15 under different strain ranges. It can be seen that the SEBS/5%MWCNTs-20/15 strain sensor could give response to strains as low as 1.0% and as high as 700%. In addition, the effect of different tensile rates (5-200 mm/min) on the dynamic strain sensing behavior was studied, as shown in Figure 7d and e. The strain range was controlled at 0-50%. The results showed that the $(R-R_0)/R_0$ of SEBS/5%MWCNTs-20/15 fiber

increased slightly with the increase of tensile rate. When the strain was increased every 100 s, $(R-R_0)/R_0$ increased rapidly with the increase of each strain, and after reaching the maximum value of each strain, $(R-R_0)/R_0$ decreased slowly with the increase of time (Figure 7f and g). The above results show that the sensor can effectively sense different levels of strain changes.

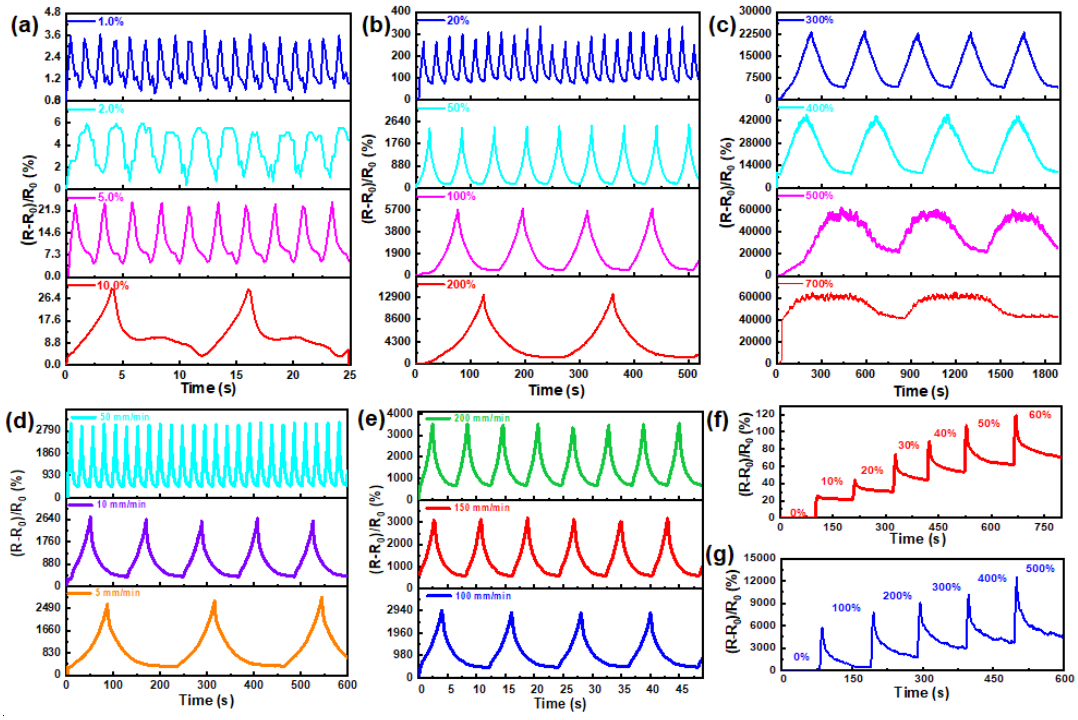

Figure 7. Dynamic response behaviors of SEBS/5%MWCNTs-20/15 sensor during stretching-releasing cycles towards strains from 0 to (a) 1.0%, 2%, 5% and 10.0%, (b) 20.0%, 50%, 100% and 200% and (c) 300%, 400%, 500% and 700%, tensile speed was 10 mm/min; Dynamic response behaviors of SEBS/5%MWCNTs-20/15 sensor during stretching-releasing cycles towards different stretching speeds of (d) 5, 10 and−50 mm/min and (e) 100, 150 and 200 mm/min, strain range was 0−50%; Dynamic response behaviors of SEBS/5%MWCNTs-20/15 sensor in the strain range of (f) 0−60%,10% strain was added every 100 s and (g) 0−500%, 100% strain was added every 100 s, tensile rate was 10 mm/min.

The current-voltage behaviour of SEBS/5%MWCNTs-20/15 strain sensors under

various tensile strains are shown in Figure 8a and b. The results showed that there was a good linear relationship between voltage and current under the load of large strains (up to 500%) and small strains (as low as 0.5%), which indicates that the strain sensor conforms to Ohm's law under different stretching conditions. Additionally, the resistance increased with increasing tensile strain, which further proved the electrical response behavior under applied strain.[47]

In order to analyze the durability of the strain sensor, 2500 stretching-releasing cycles were tested at 20% strain with a tensile speed of 10 mm/min. Figure 8c showed that the relative resistance increased slowly at the initial cycle and tended to be stable after several stretching-releasing cycles due to the continuous destruction and reconstruction of the conductive path during the stretch process.[48] The above results showed that SEBS/5%MWCNTs-20/15 strain sensor had good repeatability, stability and durability, which can be attributed to the excellent elastic properties of SEBS, as well as the strong π - π interaction between SEBS and MWCNTs.[39]

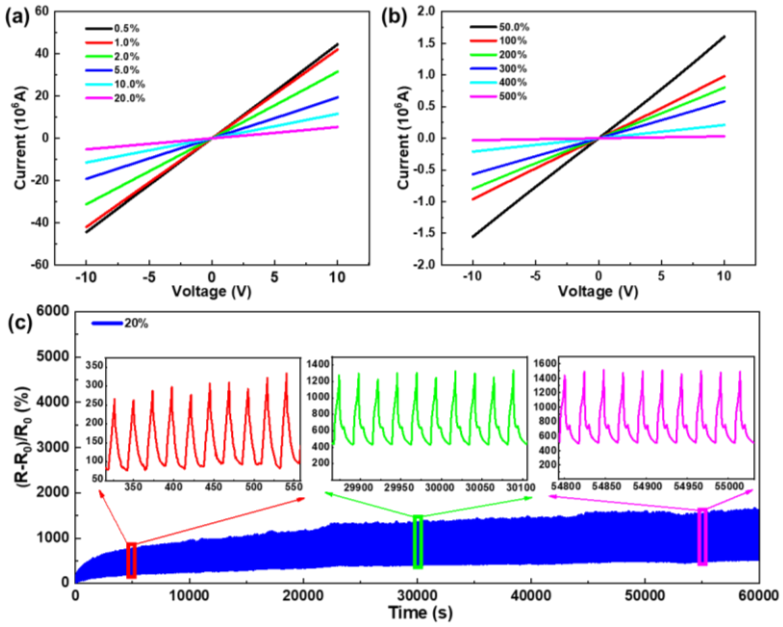

Figure 8. (a-b) Current-voltage curves under different strains for SEBS/5%MWCNTs-20/15 strain sensor; (c) Relative change of electrical resistance during 2500 tension-

release cycles at 20% strain and strain rate of 10 mm/min, the illustrations in (c) are enlarged views of the tension-release cycles at different stages.

3.4. Application

In order to demonstrate the potential application of the composite fiber in human-computer interface interaction, the SEBS/5%MWCNTs-20/15 strain sensor was installed in elbow, back of hand, neck, finger, knee and other parts to detect various human motions. The participants read and signed a consent form before conducting the experiment. Figure 9a shows the real-time monitoring of finger gesture activities. When the volunteer made different finger gestures, the SEBS/5%MWCNTS-20/15 strain sensor could give real-time response with change in resistance. When the same posture was maintained for a certain time, $(R-R_0)/R_0$ began to decline and tended to be stable immediately after reaching the maximum value, which indicates that the sensor can distinguish different movements accurately and timely.

Figure 9b shows the real-time monitoring of different elbow bending angles. It can be observed that $(R-R_0)/R_0$ increased with the increase of elbow joint bending angle and decreased with the decrease of elbow joint bending angle, indicating that different degrees of bending deformation can be sensed. Figure 9c shows the bending and stretching of index finger. The signal of the index finger bending was successfully captured by SEBS/5%MWCNTS-20/15 strain sensor. Meanwhile, the knee bending movement was tested in real time, $(R-R_0)/R_0$ rose with the bending of the knee, and the initial value was recovered after the volunteer released the knee.

The illustration in Figure 9d shows the real-time monitoring of the sitting posture of a human body, which was used to remind whether the sitting posture was correct during working or learning. When the volunteer exchanged between the correct sitting posture “a” and the wrong sitting position “b” without pause, a good response diagram was

obtained. These results showed that the SEBS/5%MWCNTs-20/15 based sensor had the ability to detect tiny and large-scale motion of human body well, and it had good application prospects in motion monitoring and artificial robot.

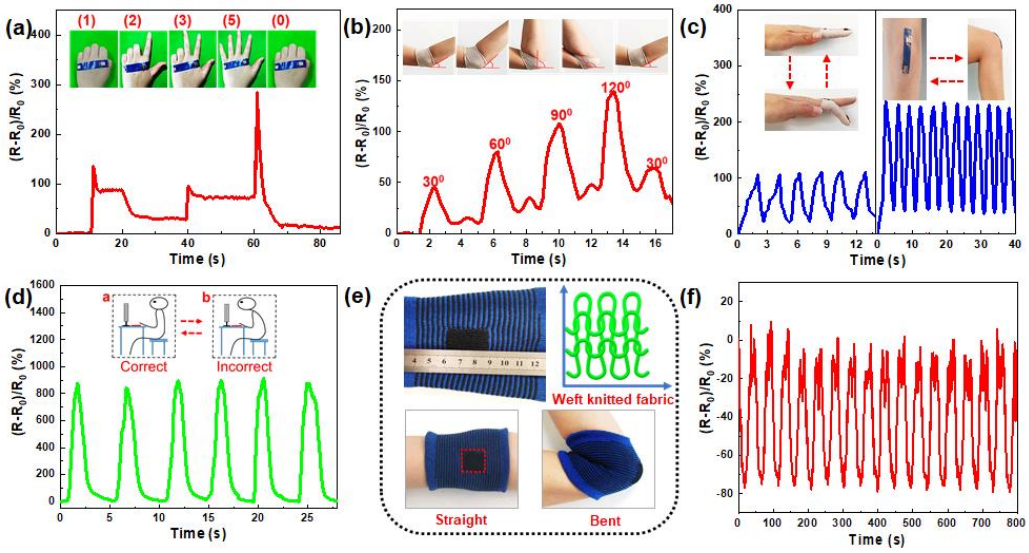

Figure 9. Human motion monitoring: (a) different gesture changes of fingers, (b) bending of elbow at different angles, (c) finger and knee extension and bending, (d) back bending; (e) knitting elbow sleeve made of SEBS/5%MWCNTS-20/15 fiber and its coil diagram, (f) change of relative resistance of elbow sleeve when elbow was straight and bent.

To further demonstrate its application, the SEBS/5%MWCNTs-20/15 fiber was made into a piece of 10 × 30 mm knitted fabric (Figure 9e). It was found that the fiber could withstand the force applied during knitting and form a continuous knitting loop. In order to enable the fabric sensor to stretch when bending and recover when straightening on the volunteer's arm, it was sewn on an elbow sleeve (Figure 9e). When the elbow changed from straight to a bending degree of 120°, the fabric could give real time change in relative resistance (0-80%) with reliable repeatability (Figure 9f); The decrease of electrical resistance was attributed that the loops in the fabric were in contact with each other when it was stretched.

4. Conclusion

In this paper, a simple and economical wet spinning method was used to prepare stretchable SEBS/MWCNTs composite fibers. The results showed that the content and aspect ratio of MWCNTs had significant effects on the morphology, mechanical property, electrical property and electromechanical property of the composite fiber. The tensile strength and elongation at break of the composite fiber decreased with the increase of MWCNTs content, while the electrical conductivity and the strain sensing range increased with increasing MWCNTs content. When the content of MWCNTs was the same, the composite fiber filled with MWCNTs of the lowest L/D ratio (SEBS/MWCNTs-1.25/15) showed the highest tensile strength and elongation at break; while the composite fiber filled with MWCNTs of the highest L/D ratio (SEBS/MWCNTs-20/15) showed the highest electrical conductivity, strain sensing range and GF. The SEBS/MWCNTs-20/15 composite fiber with 5% MWCNTs exhibited a wide working range of 0-506%, GF of 58.274 at 0% - 275% strain, and of 197.944 at 275% - 506% strain, and reliable durability. The SEBS/5%MWCNTS-20/15 composite fiber had the capability to detect different kinds of human motions, including elbow, back of hand, neck, fingers, knees and other parts, but also bear the tension applied in the weaving process to form a continuous braided ring, which can be used to detect the movement of elbow joint.

Acknowledgements

The authors thank the financial support from the National Natural Science Foundation of China (Grant no. 52003130), the Shandong Provincial Natural Science Foundation (Grant no. ZR2020QE087) and the Shandong “Taishan Youth Scholar Program” (Grant no. tsqn201909100).

Data availability

The data used to support the findings of this study are available from the corresponding author upon request.

References

1. Xu, Y.; Xie, X.; Huang, H.; Wang, Y.; Yu, J.; Hu, Z., Encapsulated core–sheath carbon nanotube–graphene/polyurethane composite fiber for highly stable, stretchable, and sensitive strain sensor. *Journal of Materials Science* **2021,** *56* (3), 1-15.
2. Cheng, Y.; Wang, R.; Sun, J.; Gao, L., A Stretchable and Highly Sensitive Graphene-Based Fiber for Sensing Tensile Strain, Bending, and Torsion. *Advanced Maters* **2015,** *27* (45), 7365-71.
3. Han, F.; Li, M.; Ye, H.; Zhang, G., Materials, Electrical Performance, Mechanisms, Applications, and Manufacturing Approaches for Flexible Strain Sensors. *Nanomaterials* **2021,** *11* (5), 1220.
4. Liu, X.; Ren, Z.; Liu, F.; Zhao, L.; Ling, Q.; Gu, H., Multifunctional Self-Healing Dual Network Hydrogels Constructed via Host-Guest Interaction and Dynamic Covalent Bond as Wearable Strain Sensors for Monitoring Human and Organ Motions. *ACS Applied Materials And Interfaces* **2021,** *13* (12), 14612-14622.
5. Li, Z.; Cheng, L.; Song, Q., An Ultra-Stretchable and Highly Sensitive Photoelectric Effect-Based Strain Sensor: Implementation and Applications. *IEEE Sensors Journal* **2021,** *21* (4), 4365-4376.
6. Zhang, S.; Zhou, Z.; Zhong, J.; Shi, Z.; Mao, Y.; Tao, H., Body-Integrated, Enzyme-Triggered Degradable, Silk-Based Mechanical Sensors for Customized Health/Fitness Monitoring and In Situ Treatment. *Advanced Science* **2020,** *7* (13), 1903802.
7. Oh, S.; Kim, J.; Chang, S. T., Highly sensitive metal-grid strain sensors via water-based solution processing. *RSC Advances* **2018,** *8* (73), 42153-42159.
8. Nie, M.; Ren, X.; Wen, L.; Han, L.; Wang, J.; Su, S., Highly Sensitive and Large Range Strain Sensor Based on Synergetic Effects with Double Conductive Layer Structures. *Sensors and Actuators A: Physical* **2021**, *318*, 112515.
9. Guo, D.; Pan, X.; Xie, Y.; Liu, Y.; He, H., Effects of service condition on the performance of conductive polymer composites for flexible strain sensors. *Sensors and Actuators A: Physical* **2021,** *318* (9), 112494.
10. Zhou, B.; Liu, Z.; Li, C.; Liu, M.; Jiang, L.; Zhou, Y.; Zhou, F.; Chen, S.; Jerrams, S.; Yu, J., A Highly Stretchable and Sensitive Strain Sensor Based on Dopamine Modified Electrospun SEBS Fibers and MWCNTs with Carboxylation. *Advanced Electronic Materials* **2021,** *7* (8), 2100233.
11. Chen, Y.; Lu, K.; Song, Y.; Han, J.; Yue, Y.; Biswas, S. K.; Wu, Q.; Xiao, H., A Skin-Inspired Stretchable, Self-Healing and Electro-Conductive Hydrogel with a Synergistic Triple Network for Wearable Strain Sensors Applied in Human-Motion Detection. *Nanomaterials* **2019,** *9* (12),1737.
12. Yu, J.; Hou, X.; He, J.; Cui, M.; Wang, C.; Geng, W.; Mu, J.; Han, B.; Chou, X., Ultra-flexible and high-sensitive triboelectric nanogenerator as electronic skin for self-powered human physiological signal monitoring. *Nano Energy* **2020,** *69* (49), 104437.
13. Han Min, S.; Asrulnizam, A. M.; Atsunori, M.; Mariatti, M., Properties of

Stretchable and Flexible Strain Sensor Based on Silver/PDMS Nanocomposites. *Materials Today: Proceedings* **2019,** *17* (P3), 616-622.
14. Chun, S.; Choi, Y.; Park, W., All-graphene strain sensor on soft substrate. *Carbon* **2017,** *116*, 753-759.
15. Wang, Y.; Li, W.; Li, C.; Zhou, B.; Zhou, Y.; Jiang, L.; Wen, S.; Zhou, F., Fabrication of ultra-high working range strain sensor using carboxyl CNTs coated electrospun TPU assisted with dopamine. *Applied Surface Science* **2021,** *566* (13), 150705.
16. Li, W.; Zhou, Y.; Wang, Y.; Jiang, L.; Ma, J.; Chen, S.; Zhou, F., Core–Sheath Fiber-Based Wearable Strain Sensor with High Stretchability and Sensitivity for Detecting Human Motion. *Advanced Electronic Materials* **2020,** *7* (1), 2000865.
17. Choi, J. H.; Shin, M. G.; Jung, Y.; Kim, D. H.; Ko, J. S., Fabrication and Performance Evaluation of Highly Sensitive Flexible Strain Sensors with Aligned Silver Nanowires. *Micromachines* **2020,** *11* (2), 156.
18. Huang, J.; Li, D.; Zhao, M.; Mensah, A.; Lv, P.; Tian, X.; Huang, F.; Ke, H.; Wei, Q., Highly Sensitive and Stretchable CNT-Bridged AgNP Strain Sensor Based on TPU Electrospun Membrane for Human Motion Detection. *Advanced Electronic Materials,* **2019,** *5* (6), 1900241.
19. Yan, C.; Wang, J.; Kang, W.; Cui, M.; Wang, X.; Foo, C. Y.; Chee, K. J.; Lee, P. S., Highly Stretchable Piezoresistive Graphene-Nanocellulose Nanopaper for Strain Sensors. *Advanced Materials* **2014,** *26* (13), 2022-2027.
20. Li, Y.; Zhou, B.; Zheng, G.; Liu, X.; Li, T.; Yan, C.; Cheng, C.; Dai, K.; Liu, C.; Shen, C.; Guo, Z., Continuously prepared highly conductive and stretchable SWNT/MWNT synergistically composited electrospun thermoplastic polyurethane yarns for wearable sensing. *Journal of Materials Chemistry C* **2018,** *6* (9), 2258-2269.
21. Cho, D.; Park, J.; Kim, J.; Kim, T.; Kim, J.; Park, I.; Jeon, S., Three-Dimensional Continuous Conductive Nanostructure for Highly Sensitive and Stretchable Strain Sensor. *ACS Applied Materials And Interfaces* **2017,** *9* (20), 17369-17378.
22. Li, H.; Du, Z., Preparation of a Highly Sensitive and Stretchable Strain Sensor of MXene/Silver Nanocomposite-Based Yarn and Wearable Applications. *ACS Applied Materials And Interfaces* **2019,** *11* (49), 45930-45938.
23. Han, J. T.; Jang, J. I.; Cho, J. Y.; Hwang, J. Y.; Woo, J. S.; Jeong, H. J.; Jeong, S. Y.; Seo, S. H.; Lee, G. W., Synthesis of nanobelt-like 1-dimensional silver/nanocarbon hybrid materials for flexible and wearable electroncs. *Scientific Reports* **2017,** *7* (1), 4931.
24. Zheng, Z.; Yao, J.; Wang, B.; Yang, G., Light-controlling, flexible and transparent ethanol gas sensor based on ZnO nanoparticles for wearable devices. *Scientific Reports* **2015**, *5*, 11070.
25. Wang, Y.; Li, W.; Zhou, Y.; Jiang, L.; Ma, J.; Chen, S.; Jerrams, S.; Zhou, F., Fabrication of high-performance wearable strain sensors by using CNTs-coated electrospun polyurethane nanofibers. *Journal of Materials Science* **2020,** *55* (26), 12592-12606.
26. Liu M.; Li Z.; Zhao X.; Young R. J.; Kinloch I. A., Fundamental Insights into Graphene Strain Sensing, *Nano Letter*. **2021**, *21,* (1), 833-839
27. Li, W.; Zhou, Y.; Wang, Y.; Li, Y.; Jiang, L.; Ma, J.; Chen, S., Highly Stretchable

and Sensitive SBS/Graphene Composite Fiber for Strain Sensors. *Macromolecular Materials and Engineering* **2020,** *305* (3), 1900736.
28. Xiang D.; Zhang X.; Harkin-Jones E.; Zhu W.; Zhou Z.; Shen Y.; Li Y.; Zhao C.; Wang P., Synergistic effects of hybrid conductive nanofillers on the performance of 3D printed highly elastic strain sensors, *Composites Part A: Applied Science and Manufacturing* **2020,** 129, 105730.
29. Zhang X.; Xiang D.; Zhu W.; Zheng Y.; Li Y., Flexible and high-performance piezoresistive strain sensors based on carbon nanoparticles@polyurethane sponges, *Composites Science and Technology* **2020,** 200:108437.
30. Wang L.; Huang X.; Wang D.; Zhang W.; Gao J., Lotus leaf inspired superhydrophobic rubber composites for temperature stable piezoresistive sensors with ultrahigh compressibility and linear working range, *Chemical Engineering Journal* **2021,** 405, 127025.
31. Qin C.; Xiang D.; Lei W.; Tang Y.; Eileen H.J.; Zhao C.; Li Y., Facile fabrication and performance of robust polymer/carbon nanotube coated spandex fibers for strain sensing, *Composites Part A Applied Science & Manufacturing* **2018,** S1359835X18302392.
32. Li, B.; Luo, J.; Huang, X.; Lin, L.; Wang, L.; Hu, M.; Tang, L.; Xue, H.; Gao, J.; Mai, Y.-W., A highly stretchable, super-hydrophobic strain sensor based on polydopamine and graphene reinforced nanofiber composite for human motion monitoring, *Composites Part B* **2020,** 181, 107580.
33. Wang, X.; Sun, H.; Yue, X.; Yu, Y.; Zheng, G.; Dai, K.; Liu, C.; Shen, C., A highly stretchable carbon nanotubes/thermoplastic polyurethane fiber-shaped strain sensor with porous structure for human motion monitoring. *Composites Science and Technology* **2018,** *168* (10), 126-132.
34. Wang, L.; Chen, Y.; Lin, L.; Wang, H.; Huang, X.; Xue, H.; Gao, J., Highly stretchable, anti-corrosive and wearable strain sensors based on the PDMS/CNTs decorated elastomer nanofiber composite. *Chemical Engineering Journal* **2019,** *362*, 89-98.
35. Ramalingame, R.; Bautista-Quijano, J. R.; Alves, D. d. F.; Kanoun, O., Temperature Self-Compensated Strain Sensors based on MWCNT-Graphene Hybrid Nanocomposite. *Journal of Composites Science* **2019,** *3* (4), 96.
36. Kashi, S.; Gupta, R. K.; Baum, T.; Kao, N.; Bhattacharya, S. N., Morphology, electromagnetic properties and electromagnetic interference shielding performance of poly lactide/graphene nanoplatelet nanocomposites. *Materials and Design* **2016,** *95*, 119-126.
37. Danish, M.; Luo, S., A New Route to Enhance the Packing Density of Buckypaper for Superior Piezoresistive Sensor Characteristics. *Sensors* **2020,** *20* (10), 2904.
38. Yu, S.; Wang, X.; Xiang, H.; Zhu, L.; Tebyetekerwa, M.; Zhu, M., Superior piezoresistive strain sensing behaviors of carbon nanotubes in one-dimensional polymer fiber structure. *Carbon* **2018,** *140*, 1-9.
39. Aleman, B.; Reguero, V.; Mas, B.; Vilatela, J. J., Strong Carbon Nanotube Fibers by Drawing Inspiration from Polymer Fiber Spinning. *ACS Nano* **2015,** *9* (7), 7392-7398.

40. Gao, Y.; Jing, H.; Zhou, Z.; Chen, W.; Shi, X., Graphene oxide-assisted multi-walled carbon nanotube reinforcement of the transport properties in cementitious composites. *Journal of Materials Science* **2019**, *55* (2) 603-618.
41. Kim, H.; Gao, S.; Hong, S.; Lee, P. C.; Kim, Y. L.; Ha, J. U.; Jeoung, S. K.; Jung, Y. J., Multifunctional primer film made from percolation enhanced CNT/Epoxy nanocomposite and ultrathin CNT network. *Composites Part B: Engineering* **2019,** *175*, 107107.
42 Pan Y.; Li L., Percolation and gel-like behavior of multiwalled carbon nanotube/polypropylene composites influenced by nanotube aspect ratio, *Polymer* **2013,** 54, 1218-1226.
43. Verma, P.; Saini, P.; Choudhary, V., Designing of carbon nanotube/polymer composites using melt recirculation approach: Effect of aspect ratio on mechanical, electrical and EMI shielding response, *Materials and Design* **2015,** 88, 269-277.
44. Kim H.; Gao S.;, Hong S.; Lee P.-C.; Kim Y. L.; Ha J. U., Sun Kyoung Jeoung S. K.; Jung Y. J., *Composites Part B* **2019,** 175, 107107.
45. Ayatollahi, M. R.; Shadlou, S.; Shokrieh, M. M.; Chitsazzadeh, M., Effect of multi-walled carbon nanotube aspect ratio on mechanical and electrical properties of epoxy-based nanocomposites. *Polymer Testing* **2011,** *30* (5), 548-556.
46. Kotsilkova, R.; Nesheva, D.; Nedkov, I.; Krusteva, E.; Stavrev, S., Rheological, electrical, and microwave properties of polymers with nanosized carbon particles. *Journal of Applied Polymer Science* **2010,** *92* (4), 2220-2227.
47. Zheng, Y.; Li, Y.; Li, Z.; Wang, Y.; Dai, K.; Zheng, G.; Liu, C.; Shen, C., The effect of filler dimensionality on the electromechanical performance of polydimethylsiloxane based conductive nanocomposites for flexible strain sensors. *Composites Science and Technology* **2017,** *139*, 64-73.
48. Duan, L.; Fu, S.; Deng, H.; Zhang, Q.; Wang, K.; Chen, F.; Fu, Q., The resistivity-strain behavior of conductive polymer composites: stability and sensitivity. *Journal of Materials Chemistry A* **2014,** *2* (40), 17085-17098.

Declaration of interests

☒ The authors declare that they have no known competing financial interests or personal relationships that could have appeared to influence the work reported in this paper.

☐The authors declare the following financial interests/personal relationships which may be considered as potential competing interests:

Author statement

We certify that all authors have seen and approved the final version of the manuscript being submitted. We warrant that the article is the authors' original work, hasn't received prior publication and isn't under consideration for publication elsewhere.